Available online at www.sciencedirect.com
SCIENCE DIRECT®
Journal of Power Sources 145 (2005) 667–674
JOURNAL OF POWER SOURCES
www.elsevier.com/locate/jpowsour

Bi_2O_3–WO_3 compounds for photocatalytic applications by solid state and viscous processing

A.P. Finlayson [a,b,*], E. Ward [a,b], V.N. Tsaneva [a], B.A. Glowacki [a,b]

[a] *Department of Materials Science and Metallurgy, University of Cambridge, Pembroke Street, Cambridge CB2 3QZ, UK*
[b] *IRC in Superconductivity, Cavendish Laboratories, University of Cambridge, Madingley Road, Cambridge CB3 0HE, UK*

Accepted 10 January 2005
Available online 14 April 2005

Abstract

Water-splitting photoelectrochemical cells utilising photocatalysts have the potential to become a significant hydrogen source for fuel cells. Historically, the photocatalytic properties of TiO_2 and other compounds have been carefully investigated, but they suffer from poor energy conversion efficiencies for solar radiation.

Inspired by the low bandgaps and high electrical conductivities of WO_3 and Bi_2O_3, this study investigates the suitability of compounds within this binary system as efficient photocatalysts. The structure and optical absorption spectra of these compounds have been determined via X-ray diffraction and UV–vis spectroscopy over the range of 300–900 nm.

The semiconductor bandgaps of Bi_2O_3, WO_3 and Bi_2WO_6 were found to be 0.2 eV, in agreement with previously reported results. Two sample preparation techniques have been considered—solid-state processing and viscous processing techniques. A custom-built, computerised micro-coextrusion system has been used to prepare intermediate compounds from the WO_3–Bi_2O_3 binary oxide system and the design and optimisation of this technique are discussed.

Keywords: Photocatalysis; Tungsten oxide; Bismuth oxide; Hydrogen production

1. Introduction

As hydrogen-based power and transportation technologies develop the need for an effective hydrogen source to power fuel cells in the hydrogen economy becomes evident. In the current climate, potential hydrogen sources should entail neither the expense of excessive energy consumption nor the environmental impact of greenhouse gas emissions. Hydrogen from photoelectrochemical cells is believed to offer the prospect of such a source.

Photocatalytic water splitting by n-type TiO_2 under UV illumination was first reported over 30 years ago by Fujishima and Honda [1]. Since then a number of other photocatalytic compounds have been investigated with the aim of improving catalyst activity and stability in the irradiated aqueous environment. In 2001 Zou et al. first demonstrated the direct splitting of water by visible light over an $In_{1-x}Ni_xTaO_4$ photocatalyst [2].

As energy conversion devices, water-splitting photoelectrochemical cells convert photon energy to the Gibbs free energy of hydrogen and oxygen via excited electron states in the photocatalyst. These excited electron states result from the promotion of a valance band electron to a level above the conduction band edge on the absorption of an incident photon. In practice, any energy in excess of the bandgap energy will be dissipated as heat since electrons promoted to higher states readily thermalise to the conduction band edge. Analysis of the solar spectrum [3] (Fig. 1) shows that the maximum absorption of energy that can be used to catalyse electrochemical reactions will be observed if the semiconductor bandgap is 1.7 eV. This energy is greater than the 1.23 eV necessary for the water-splitting reaction to proceed under standard conditions and

* Corresponding author. Tel.: +44 1223 334375; fax: +44 1223 334373.
E-mail address: apf23@cam.ac.uk (A.P. Finlayson).

0378-7753/$ – see front matter © 2005 Elsevier B.V. All rights reserved.
doi:10.1016/j.jpowsour.2005.01.072

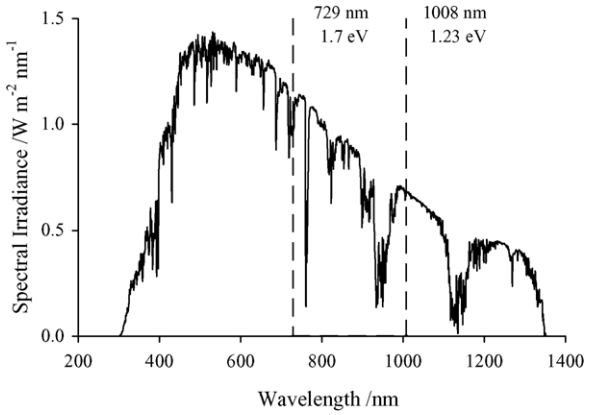

Fig. 1. The spectral distribution of solar radiation under air mass 1.5 conditions when the sun is 48.81° above the horizon. The maximum useful energy conversion by a semiconductor photocatalyst occurs for a bandgap of 1.7 eV whilst 1.23 eV are required for the water-splitting reaction to proceed.

may allow bridging of the reaction electrochemical potentials.

Recently, the compound Bi_2WO_6 has been observed to photocatalyse both the evolution of oxygen from aqueous silver nitrate under visible light illumination and the mineralization of organic compounds ($CHCl_3$ and CH_3CHO) [4]. It has a bandgap of 2.69 eV. The phase relations the Bi_2O_3–WO_3 system were described by Speranskaya [5] (see Fig. 2).

There are five intermediate oxides exhibiting a range of structures with the compositions: $Bi_2W_2O_9$, Bi_2WO_6, Bi_4WO_9, Bi_6WO_{12} and $Bi_{12}WO_{21}$. The focus of this research has been to investigate the solid-state preparation of intermediate oxides to assess their potential as candidate photocatalyst compounds.

A secondary aim of this study has been to develop microcoextrusion process to accelerate sample manufacture and

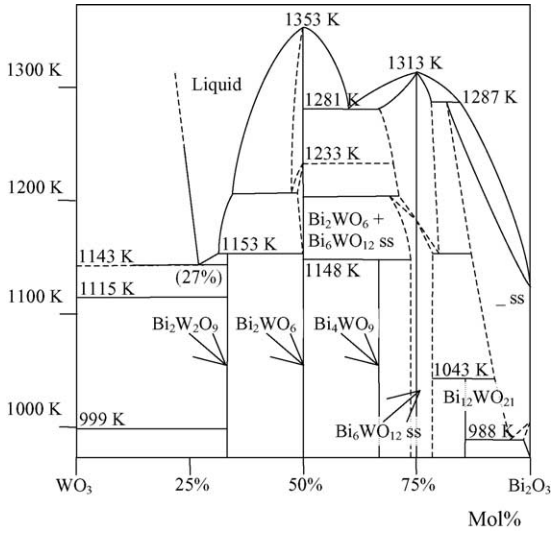

Fig. 2. Bi_2O_3–WO_3 system phase diagram following Speranskaya [5]. There are intermediate oxides of fixed composition and one solid solution range. Dashed lines indicate metastable states.

improve quality compared to the conventional solid-state processing route. The viscous sample based process allows the testing of a larger number of different compositions when mapping a new phase diagram or investigating the effect of impurities on a property such as photocatalytic activity.

2. Experimental

2.1. Materials and sample preparation

The Bi_2O_3 and WO_3 mixed oxides were prepared via the interaction of pure Bi_2O_3 and WO_3 powders at temperatures higher than 1070 K.

One set of samples was prepared by conventional solid-state processing techniques. Stoichiometric mixtures of Bi_2O_3 and WO_3 as-received powders were ground together and formed into compact pellets. The pellets were heated to 1003 K for 1 h followed by 1 h at 1213 K for all samples except the pure Bi_2O_3 (Bi_2O_3):2(WO_3) which were heated to a maximum temperature of 1073 K. Segments of these pellets taken before heating were used for DTA characterisation.

A second set of viscous samples were prepared from Bi_2O_3 and WO_3 powders that had been milled for 192 h. The separate powders were suspended in acetone with a dispersant (Dispex) and ball milled using 8 mm alumina beads before filtering through a 35 μm nylon mesh and drying in air. A (Bi_2O_3):(WO_3) stoichiometric mixture of these milled powders was combined with glycerol (analytical grade, 12% by mass) to give a viscous paste that was then evenly coated onto alumina (Al_2O_3), platinum and strontium titanate ($SrTiO_3$) bases before heating to 1173 K for 10 h. Tungsten foil was heated in air to the reaction temperature so that its suitability as a base material could be assessed.

An alumina tube furnace was used to heat all the samples under an oxygen atmosphere allowing a maximum heating rate of 200 K h^{-1} and slow cooling in air to room temperature.

2.2. Sample characterisation techniques

A Jeol 5800LV SEM was used in both backscattered and energy dispersive X-ray (EDX) detection modes. An accelerating voltage of 20 keV was used with a chamber pressure of 31 Pa (low vacuum mode) to prevent sample charging.

Measurement of the volume averaged particle diameter was performed using a Malvern Mastersizer 4000.

A Stanton Redcroft, STA 780 differential thermal analyser/thermogravimetric analyser and alumina sample holders were used for all thermal analyses. A constant flow-rate of 50 ml min^{-1} $O_{2(g)}$ was passed over the samples throughout each 2 K min^{-1} heating program. The maximum analysis temperature was selected for each sample to be 50 K below the melting point for the stoichiometric oxide formed by that composition as predicted by the phase diagram (Fig. 2).

Powder X-ray diffraction patterns were measured using a Philips PW1050 X-ray Diffractometer in the Bragg-Bretano geometry with unfiltered Cu Kα radiation. A divergence

Table 1
EDX compositional analysis of Bi_2O_3 and WO_3 performed before and after ball milling with alumina beads

	Bi (at.%)	W (at.%)	Al (at.%)	O (at.%)	100 × (Al (at.%)/*X* (at.%))
Bi_2O_3 as-received	68.5	–	1.6	29.9	2.3
Bi_2O_3 milled	62.9	–	0.7	36.4	1.1
WO_3 as-received	–	29.1	0.9	70.0	3.2
WO_3 milled	–	25.8	1.5	72.7	5.8

X denotes the dominant metallic element: Bi for Bi_2O_3 samples and W for WO_3 samples.

and anti-scatter slit of 1/2° were used in conjunction with a 0.2 mm receiving slit and collection time of 2 s for each 0.05° step. Where appropriate data were available in the literature both the relative intensity ratio method and the Rietveld algorithms as described by Wiles and Young [6] and implemented in the Phillips X'Pert software package were used to calculate the sample composition from X-ray diffraction data.

A Uvikon Kontron 860 UV–vis spectrophotometer without an integrating sphere was used to collect absorption spectra in transmission mode. Samples were prepared by dilution to between 5 and 15% by mass in dry potassium bromide and formed into pellet under a pressure of 7.5 MPa. Determination of the position of the optical absorption edge and, therefore, the semiconductor bandgap was based upon the method described by Fochs [7]. The measured absorbance was referenced to pure potassium bromide and transmittance (*T*) values were calculated from this using the Beer–Lambert law. Assuming $(1 - T)$ gives an approximation to the sample reflectivity the onset of the absorption edge was indicated by low wavelength/high energy limit of the linear region of a plot of reflectivity against photon energy.

3. Results

3.1. Precursor preparation and characterisation

The morphology of the Bi_2O_3 and WO_3 powders before and after milling may be observed from the SEM micrographs. Particle size analysis showed that the volume averaged mean diameter of the Bi_2O_3 particles decreased from 26.8 to 4.5 μm whilst the milled particles are more angular and show less agglomeration (Fig. 3). The volume averaged mean diameter of the WO_3 particles also decreased from 66.6 to 7.9 μm this decrease in particle size is clearly illustrated by Fig. 4. A significant number of fine particles sized between 0.1 and 1 μm were observed in both milled samples but in neither of the as-received samples.

The results of EDX analysis performed before and after milling are presented in Table 1. It can be seen that the Al content of the Bi_2O_3 particles decreases after milling whilst the Al content of the WO_3 particles increases by 81% from 3.2 to 5.8 at.%. A non-stoichiometric concentration of oxygen has been measured in all the samples. This may be attributed to the increased absorption of lower energy X-rays, such as the 0.523 eV characteristic of oxygen, compared to that of higher energy X-rays by the porous sample surface.

3.2. Phase formation in the Bi_2O_3–WO_3

The DTA traces obtained from pressed powder pellets of Bi_2O_3, Bi_2O_3 and mixed powders are presented in Fig. 5. There are a number of features which may be observed. First, the trace for pure WO_3 shows an endothermic peak a 1028 K which may be attributed to the polymorphic transition reported by Speranskaya [5]. Pure Bi_2O_3 exhibits an en-

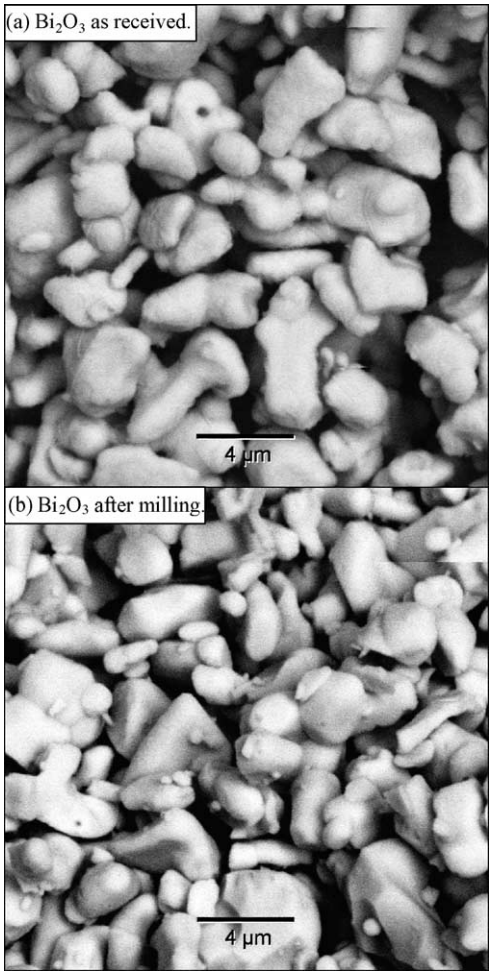

Fig. 3. SEM backscattered micrographs of Bi_2O_3: (a) as-received from supplier (scale bar measures 4 μm); (b) following 192 h ball milling with 8 mm alumina beads (scale bar measures 4 μm).

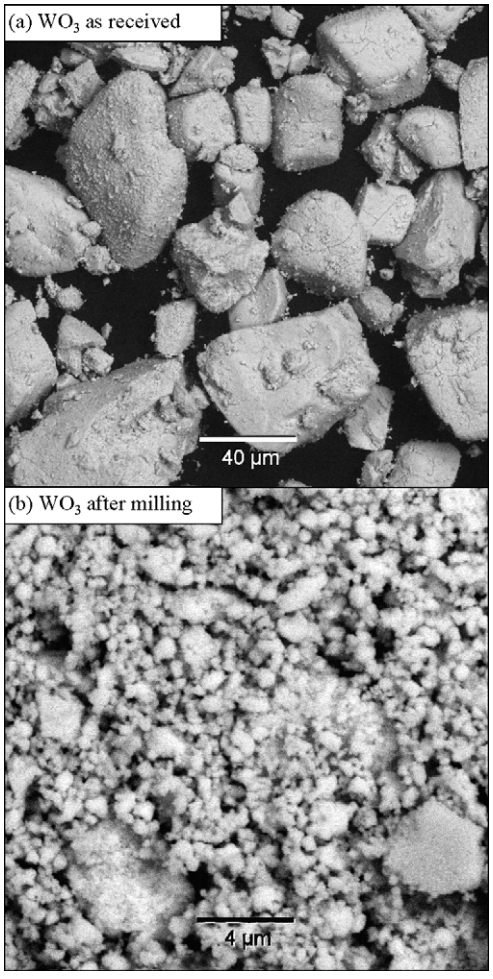

Fig. 4. SEM backscattered micrographs of WO_3: (a) as-received from supplier (scale bar measures 40 μm); (b) following 192 h ball milling with 8 mm alumina beads (scale bar measures 4 μm).

dothermic transition from the α to β structure at 1073 K. This feature may also be observed in the data for the mixed samples: 2(Bi_2O_3):(WO_3), 3(Bi_2O_3):(WO_3) and 6(Bi_2O_3):(WO_3), indicating the continued presence of α-Bi_2O_3 at 1073 K.

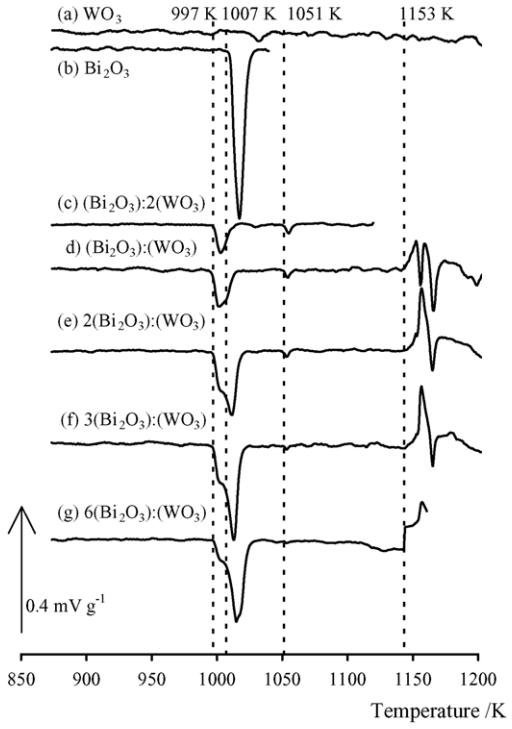

Fig. 5. DTA traces (mass normalised and background subtracted) from pressed pellets of: (a) pure WO_3; (b) pure Bi_2O_3; (c) 1(Bi_2O_3):2(WO_3) mixed; (d) 1(Bi_2O_3):1(WO_3) mixed; (e) 2(Bi_2O_3):1(WO_3) mixed; (f) 3(Bi_2O_3):1(WO_3) mixed; (g) 6(Bi_2O_3):1(WO_3) mixed. The inter-diffusion of Bi_2O_3 and WO_3 (997 K), α → β transition in Bi_2O_3 (1007 K) and reactions at 1051 and 1153 K are observed. Dotted lines indicate the onset temperatures of thermal events of interest.

Three other features of interest may be observed in the data from the mixed samples.

A sharp endothermic peak with an onset temperature of 997 K reflects the initial interdiffusion of Bi_2O_3 and WO_3. Although it partially overlaps the Bi_2O_3 α to β transition, it can be seen that the area of this peak is the greatest in those samples in which the ratio mol(Bi_2O_3):mol(WO_3) is the closest to unity. This implies a greater area of contact between particles of different compositions and, therefore, an increased diffusive flux.

Table 2
Phase quantification and Bi/W elemental ratio derived from the powder X-ray diffraction patterns of $x(Bi_2O_3):y(WO_3)$ solid-state processing samples following heating

Sample $x(Bi_2O_3):y(WO_3)$	Compound	X-ray reference pattern JCPDS #	Composition by mass (%)	Bi (at.%)/W (at.%)
(Bi_2O_3):2(WO_3)	Bi_2WO_6	79-2381	83.5 ± 0.6	2.2
	$Bi_7WO_{13.5}$	85-1286	12.1 ± 0.4	
	$Bi_2W_2O_9$	33-0221	4.4 ± 0.6	
(Bi_2O_3):(WO_3)	Bi_2WO_6	79-2381	100	2
2(Bi_2O_3):(WO_3)	$Bi_{24}WO_{39}$	43-0447	78.8 ± 5	8.8
	Bi_2WO_6	79-2381	21.2 ± 5	
3(Bi_2O_3):(WO_3)	$Bi_7WO_{13.5}$	85-1286	88.4 ± 0.9	5.7
	Bi_2WO_6	79-2381	11.6 ± 0.6	
6(Bi_2O_3):(WO_3)	$Bi_{24}WO_{39}$	43-0447	84.1 ± 5	16.7
	$Bi_7WO_{13.5}$	85-1286	14.5 ± 5	
	Bi_2WO_6	79-2381	1.4 ± 5	

Both the relative intensity ratio method and Rietveld analysis have been used following the availability of published I/I_{corr} values or structural data.

Another endothermic peak onset occurs at 1051 K in samples: (Bi_2O_3):2(WO_3), (Bi_2O_3):(WO_3) and 2(Bi_2O_3):(WO_3). The area of this feature is correlated with the presence of Bi_2WO_6 and, consequently, it is thought to indicate a transition between different structures of this compound.

Finally, a complex set of features are observed with an onset temperature of 1153 K. They are believed to represent the conversion of the initial interdiffusion products to the equilibrium phase at that temperature and will be the subject of further investigation.

3.3. Solid-state processing

3.3.1. Characterisation of solid-state samples

Compositional analyses of the samples prepared via conventional processing techniques are presented in Table 2. It can be seen that only one sample, (Bi_2O_3):(WO_3), reacted completely to form a single reaction product. The other samples contain significant levels of both tungsten rich and bismuth rich phases relative to their stoichiometry, indicating the presence of regions of partially reacted material.

Samples (Bi_2O_3):(WO_3) and 3(Bi_2O_3):(WO_3) exhibit an overall ratio of bismuth atoms to tungsten atoms in each sample close to that predicted by considering the sample stoichiometries. Sample (Bi_2O_3):2(WO_3) is tungsten poor, indicating a loss of the low melting point compound $Bi_2W_2O_9$ during the heating process. Samples 2(Bi_2O_3):(WO_3) and 6(Bi_2O_3):(WO_3) contain high levels of the compound $Bi_{24}WO_{39}$ which is formed from the metastable β solid solution of tungsten in Bi_2O_3. Consequently, the elemental composition of this compound cannot be defined exactly from the measured data and, therefore, deviations in the overall elemental fractions may be anticipated.

3.3.2. Characterisation of optical properties

UV–vis absorption spectra measured for selected samples are presented in Fig. 6. The variation in magnitude of the absorbance is influenced by both the concentration of the sample in potassium bromide and the absorbance of the sample compound. All samples show strong absorbance in the region 550–800 nm. When considering transmission mode measurements on a powder this indicates high reflectivity leading to a significant deflection of intensity from the straight-through beam to larger angles such that it is not collected by the detector.

Fig. 7 shows the relationship between the estimated sample reflectivity and photon energy. It can be observed that for all samples the high energy limit of the linear region of the curve is approximately 2.6 ± 0.2 eV.

3.4. Viscous processing

3.4.1. Preparation of viscous samples

The (Bi_2O_3):(WO_3) viscous samples were characterised by X-ray diffraction. As can be seen from Fig. 8, Bi_2WO_6 is the majority phase in all three samples. The samples heated upon alumina and strontium titanate bases match the reference pattern most closely, only one peak remaining unidentified. Three unidentifiable peaks are present in the sample prepared upon a platinum base. They are of low relative intensity and may reflect the poorer counting statistics of this diffraction trace.

In addition to this, it was observed that the samples prepared upon alumina and strontium titanate decreased in mass by 13.2 ± 0.5 and 10.9 ± 1.7%, respectively. This is consistent with complete vaporisation of the glycerol component

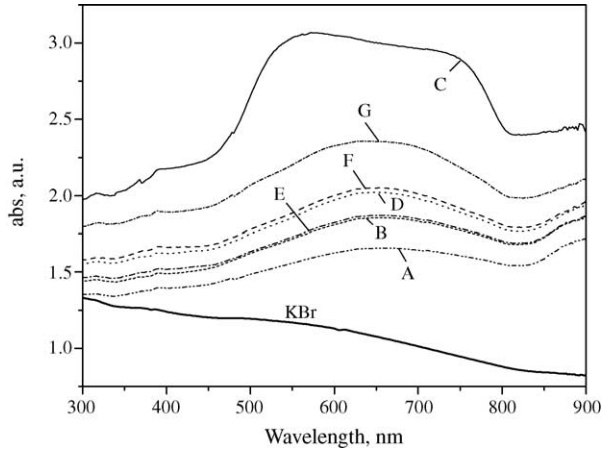

Fig. 6. UV–vis absorption spectrum measured for samples diluted by potassium bromide: (A) 5% Bi_2WO_6; (B) 10% Bi_2WO_6; (C) 15% Bi_2WO_6; (D) 5% Bi_2O_3 as-received; (E) 5% WO_3 as-received; (F) 5% $Bi_{24}WO_{39}$ (purity 84% from sample 6(Bi_2O_3):(WO_3), heated); (G) 5% $Bi_7WO_{13.5}$ (purity 88% from sample 3(Bi_2O_3):(WO_3), heated); 5% Bi_2WO_6. A measured potassium bromide reference spectrum (KBr) is displayed for comparison.

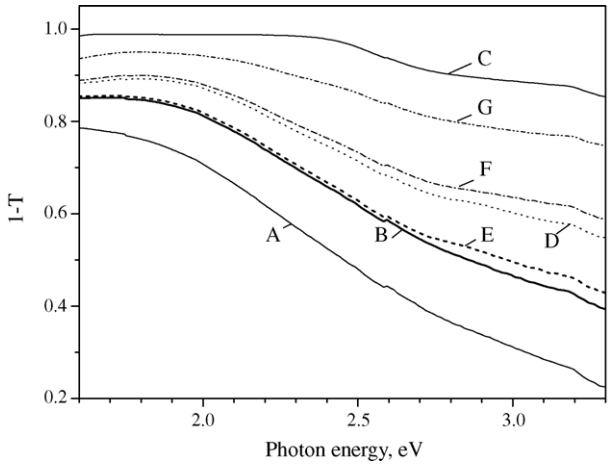

Fig. 7. Plot of the reflectivity (estimated as $(1 - T)$) against photon energy for: (A) 5% Bi_2WO_6; (B) 10% Bi_2WO_6; (C) 15% Bi_2WO_6; (D) 5% Bi_2O_3 as-received; (E) 5% WO_3 as-received; (F) 5% $Bi_{24}WO_{39}$ (purity 84% from sample 6(Bi_2O_3):(WO_3), heated); (G) 5% $Bi_7WO_{13.5}$ (purity 88% from sample 3(Bi_2O_3):(WO_3), heated); 5% Bi_2WO_6. The high energy limit of the linear region may be observed to be approximately 2.6 eV for each sample.

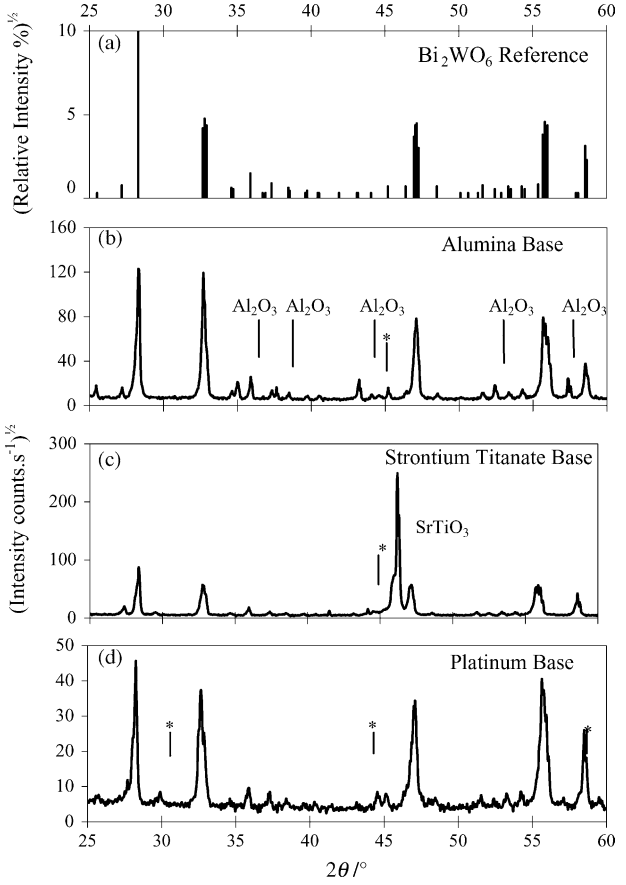

Fig. 8. X-ray diffraction patterns for: (a) Bi_2WO_6 (JCPDS #79-2381); (b) (Bi_2O_3):(WO_3)/glycerol heated on an alumina base; (c) (Bi_2O_3):(WO_3)/glycerol heated on a strontium titanate base; (d) (Bi_2O_3):(WO_3)/glycerol heated on a platinum base. "Al_2O_3" denotes peaks matching JCPDS #82-1399. "$SrTiO_3$" denotes the (2 0 0) reflection from JCPDS #86-0178. "*" denotes peaks which could not be assigned to a reference pattern.

of a viscous sample. The sample on a platinum base delaminated and separated from the substrate during the heating and decreased in mass by $22.8 \pm 0.3\%$. This large decrease in mass may be partly attributed to the loss of material as a result of this separation from the platinum substrate.

3.4.2. Micro-coextrusion

The computer controlled micro-coextrusion system developed for this project is presented in Fig. 9. It comprises of an extrusion head connected to an array of syringes containing the component viscous samples. Stepper motors independently depress the piston of each syringe whilst the position of the extrusion head in the *x*, *y* plane is controlled by custom-written software. System calibration is achieved by measuring the mass deposited per step, the concentration of the compound of interest in the viscous sample, and the density of the viscous samples. This allows the number of steps required to extrude a sample of specified volume and bulk composition to be calculated.

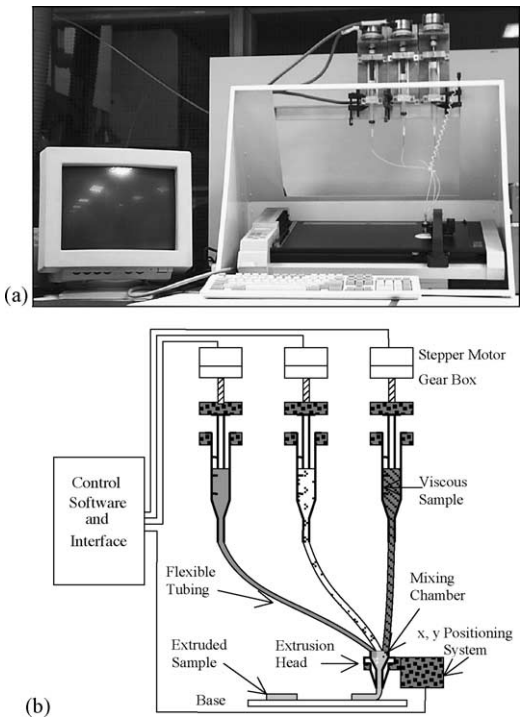

Fig. 9. The micro-coextruder system: (a) photograph of custom-built system; (b) schematic showing major components of system.

4. Discussion

4.1. Solid-state processing of bismuth tungsten oxides

Differential thermal analysis of bismuth tungsten oxides is in broad agreement with previously published thermodynamic data. The onset of inter-diffusion occurs at 997 K whilst the sharp endothermic peak shape suggests that reaction is rapid. However, the presence of complex features at 1153 K and the phase analysis of those samples heated to 1173 K for 10 h indicate that the exact explanation is more complex than this. Poor mixing of the precursors increases the distance over which diffusion must occur for complete reaction and also decreases the surface area of contact between particles of different compositions, as does a large particle size. Control of these two factors will decrease the length of time required for complete reaction to occur.

Ball milling with alumina beads is a suitable technique for reducing the particle of Bi_2O_3 and WO_3 precursor powders for synthesizing bismuth tungsten oxide. Particle sizes may be reduced to less than 10 μm without large-scale transfer of material from the milling media which might otherwise form a significant source of impurities in the final product. The increase in the number of particles sized between 0.1 and 1 μm observed after milling will increase the rate of inter-diffusion further.

The importance of thermal analysis in determining the correct heat treatment is emphasised by the variations in the ratio of bismuth to tungsten in the conventionally processed samples. If the temperature chosen is too

high then the more volatile reactants and products are depleted this is observed in the (Bi_2O_2):2(WO_3) sample. Conversely, rapid cooling may result in high temperature phases such as solid solutions being 'frozen in' at room temperature, avoiding transitions to the intended reaction product as observed in the samples 2(Bi_2O_2):(WO_3) and 6(Bi_2O_2):(WO_3).

Alumina is the most suitable base to use for heating bismuth oxide and tungsten oxide to 1173 K as no lack of contact between sample and base was observed and the X-ray diffraction pattern of the final product most closely approximates the reference pattern of Bi_2WO_6, the intended reaction product. Despite its elemental compatibility, the rapid oxidation of metallic tungsten at the temperatures of interest mean that it is not suitable for use as a base material.

4.2. Characterisation of optical properties

Analysis of the UV–vis absorption spectra provided a value of 2.6 ± 0.2 eV for the semiconductor bandgap of the samples. This is consistent with the values from the published literature of 2.6 eV for α-Bi_2O_3 [8], 2.6 eV for WO_3 [9] and 2.69 eV for Bi_2WO_6 [4].

Major contributions to the uncertainty in the bandgap follow from the simplifying assumptions made in the estimation of the reflectivity and also from the distortion of the absorption spectrum resulting from dilution in a transparent reference medium. This latter effect may be observed by comparing the curves obtained from Bi_2WO_6 at different dilutions in Fig. 6. A UV–vis spectrophotometer incorporating an integrating sphere collects light reflected to all angles and negates then need for sample dilution thus improving the accuracy of the measurement.

4.3. Viscous processing via micro-coextrusion

A number of different factors were considered in the design of the micro-coextrusion system so that both the requirements specific to viscous processing and for successful solid-state processing could be met.

Considerations specific to viscous processing centre upon need to ensure compositional accuracy and correctly sequence the steps required to extrude a sample.

Compositional accuracy requires that consecutive samples do not contaminate each other, that the variation in the quantity of each component extruded per step in small and that there is no residue of the liquid fraction remaining in the final, heated samples. A cleaning routine whereby the extrusion head is flushed with pure glycerol followed by sample of the desired composition extruded to waste is implemented in the micro-coextrusion procedure to minimise sample contamination whilst calibration procedures allow measurement of the variation in viscous sample mass extruded per step. The viscous samples heated upon alumina and strontium titanate exhibited in mass decreases during heating consistent with the complete volatilisation of their glycerol component.

Sequencing of the extrusion steps is complicated by the mechanical hysteresis exhibited by the syringe and tubing assemblies. This can be minimised through the use of glass syringes and decreased tubing lengths but still requires study in order to model this aspect of the system's behaviour in the computer control software.

The preparation of samples using conventional solid-state processing techniques has highlighted three important issues: careful choice of heat treatment temperature; a relatively rapid, well controlled transformation to the desired product, and sample cohesion. When applied to the micro-coextrusion these issues imply a number of limitations.

First, unless the effect of temperature a variable under investigation the compositions of samples extruded onto a common base must be carefully chosen to allow simultaneous heating of the samples. Preliminary thermal analysis of the sample components before extrusion offers a way to control this.

Ensuring a rapid and well controlled reaction means that the particle sizes of the solid component of the viscous samples must be chosen to maximise the cross-section for diffusion and minimise the diffusion distance required for complete reaction. A low liquid fraction is desirable in order to maximise the density of the final samples but the viscous samples must be sufficiently fluid for good mixing to occur during the extrusion process. It is possible that further mechanical agitation will be necessary to supplement this. Finally, the viscous samples should be sufficiently viscous not to flow under their own weight following deposition.

The flexibility of computer control means that it is possible to extrude samples both as a spiral or cross-hatch pattern of constant composition or as a line of continuously varying composition depending upon the requirements of subsequent characterisation techniques.

5. Conclusions

The thermal analysis performed during the course of this investigation has allowed identification of specific phase transitions and reactions within the Bi_2O_3–WO_3 system. However features observed at higher temperatures need further investigation including high temperature X-ray diffractometry to fully explain the observed thermal events.

From preliminary work we can conclude that other compounds in the Bi_2O_3–WO_3 phase system show similar optical properties to Bi_2WO_6 so also have the potential to exhibit photocatalysis. $Bi_7WO_{13.5}$ and $Bi_{24}WO_{39}$ are of particular interest because their broad tungsten solubility ranges open up the possibility of further optimisation.

Independent of these positive results, none of the measured values for the semiconductor bandgaps approach 1.7 eV that

would be required for maximum solar energy conversion. Therefore, a wider range of oxide compositions must be investigated for water-splitting photocatalysts to operate at economic efficiencies. This extended search will entail screening of a large number of candidate compounds photocatalytic potential.

Although there are still practical challenges to be overcome, micro-coextrusion as a viscous processing technique offers potential benefits over solid-state processing for the fabrication of numerous samples. Automated sample preparation has the potential to accelerate the optimisation of material properties. In the case of high activity photocatalysis it facilitates the search for maximum energy conversion efficiency.

However, accurate and efficient sample characterisation is also necessary for the benefits of rapid synthesis to be realised. For this reason the accurate determination of optical properties through the use of a UV–vis spectrophotometer incorporating an integrating sphere will be essential.

Acknowledgements

The authors acknowledge the assistance of E.A. Robinson and R.J. Stern with the development of the micro-coextrusion system. A.P. Finlayson acknowledges the support of the Engineering and Physical Sciences Research Council (EPSRC).

References

[1] A. Fujishima, K. Honda, Nature 238 (1972) 37.
[2] Z. Zou, J. Ye, K. Sayama, H. Arakawa, Nature 414 (2001) 625–627.
[3] Standard Tables for Reference Solar Spectral Irradiances: G173-03, ASTM, 2003.
[4] J. Tang, Z. Zou, J. Ye, Catal. Lett. 92 (2004) 53–56.
[5] E.I. Speranskaya, Neorg. Mater. 6 (1970) 149–151.
[6] D.B. Wiles, R.A. Young, J. Appl. Crystallogr. 14 (1981) 149–151.
[7] P.D. Fochs, Proc. Phys. Soc. B69 (1956) 70.
[8] J.M. Carlsson, B. Hellsing, H.S. Domingos, P.D. Bristowe, Phys. Rev. B 65 (2002), Art. No. 205122.
[9] A.A. Likalter, Physica B 315 (2002) 252–260.